PROCEEDINGS, 49th Workshop on Geothermal Reservoir Engineering
Stanford University, Stanford, California, February 12-14, 2024
SGP-TR-227

Analytical Estimates on the Deep Aquifer Thermal Energy Storage Using Electromagnetic Heating

Samuel O. de Almeida[1], Pacelli L. J. Zitha[2] and Grigori Chapiro[3]

[1] Federal Institute of Southeast Minas Gerais, Brazil

[2] Delft University of Technology (TUD), Netherlands

[3] Federal University of Juiz de Fora (UFJF), Brazil

samuel.oliveira@ifsudestemg.edu.br, p.l.j.zitha@tudelft.nl, grigori@ice.ufjf.br

Keywords: ATES, low-enthalpy geothermal sources, electromagnetic heating, flows in porous media, partial differential.

ABSTRACT

Electromagnetic (EM) heating is a promising approach for the efficient storage of renewable energy derived from sources like photovoltaic solar and wind power within aquifers. In this study, we delve into the dynamics of how this captured energy elevates the temperature of a representative deep aquifer over a six-month period, as well as the extent to which this stored energy can be subsequently recovered during the following six months.

Our approach involves injecting water into the aquifer at a constant flow rate while concurrently subjecting it to high-frequency electromagnetic microwaves generated at the water's natural resonance frequency of 2.45 GHz. To comprehensively describe this intricate interplay between reservoir flow and EM heating, we employ Darcy's and energy balance equations. Notably, the energy balance equation incorporates a source term to account for the propagation and absorption of EM waves, which are modeled independently using Maxwell's equations. For a more simplified model, we analytically solve these equations.

The analytical estimates are rigorously benchmarked against numerical simulations, utilizing data from prior controlled laboratory experiments documented in the literature. Our results demonstrate the considerable efficacy of down-hole EM heating as an innovative method for storing renewable energies, offering a viable solution to mitigate the inherent intermittency associated with these sources. This research contributes to the evolving landscape of sustainable energy storage solutions.

1. INTRODUCTION

In the past decade, the significance of solar and wind energy has grown significantly due to societal pressure to reduce CO_2 emissions from natural hydrocarbon use. However, the intermittent nature of solar and wind energy poses a challenge, as their peak generation times do not align with the high energy consumption periods in buildings, especially during colder seasons Dorsey-Palmateer (2019).

To address this issue, Aquifer Thermal Energy Storage (ATES) stores heated water in the subsurface, enhancing the efficiency of the terrestrial energy system Dickinson et al., (2009). ATES involves cyclic operations between summer and winter, extracting cold water in summer for cooling and reinjecting it in the aquifer, while in winter, the process is reversed for heating Sommer (2015). Hybrid energy systems, combining low enthalpy geothermal sources with wind or solar energy, have been explored for increased efficiency Kastner et al., (2017), Lau et al., (2019). However, there is a lack of data and models for high-depth applications.

Recently, subsurface Electromagnetic (EM) heating was introduced as a novel approach for energy storage in deep aquifers Almeida et al., (2022)a, see Fig. 1. Unlike traditional methods, EM heating is less affected by reservoir heterogeneity, allowing uniform heat distribution Cerutti et al., (2013). Experiments have shown faster and more efficient heating than traditional methods, with reduced thermal losses Eskandari et al., (2015), Jha et al., (2011), Mukhametshina and Martynov (2013). However, the impact of EM propagation on energy storage efficiency and the role of various energy losses in the context of geothermal sources remain less understood. Previous studies on EM heating focused on polluted soil cleanup and enhanced oil recovery Bera and Babadagli, (2015), Chhetri and Islam (2008), Hasanvand and Golparvar (2014), Paz et al., (2017), Pizarro and Trevisan (1990), Sahni et al., (2000), Shafiai and Gohari (2020). The present paper aims to explore these aspects, considering deep reservoirs and the potential for increased renewable energy usage.

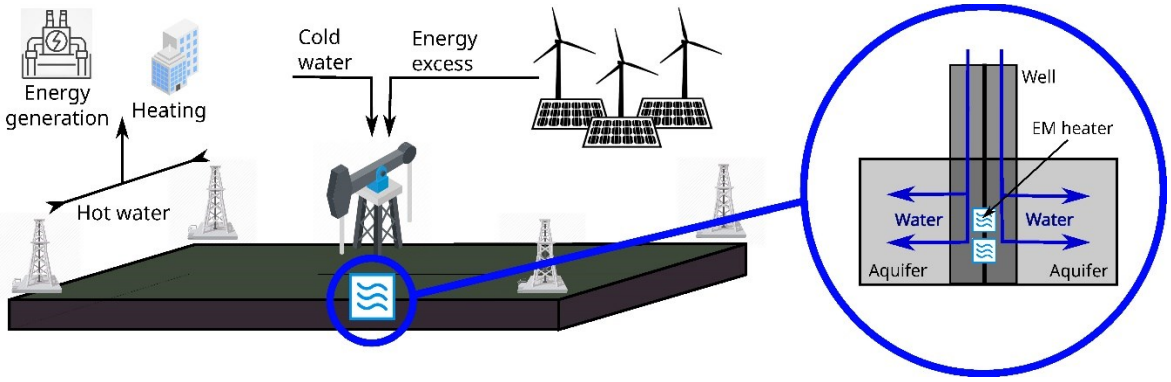

Figure 1: Schematic representation of Electromagnetic-assisted Water Flooding.

The present paper focuses on developing the analytical solution for a simplified model describing high-temperature ATES. Analytical solutions are of scientific interest because they reveal, more generally than empirical numerical simulations, the relationships between system parameters and outcomes of interest, such as the thermal recovery efficiency Tang and Rijnaarts (2023).

We organized the paper as follows. Section 2 provides the mathematical model. Section 3 presents an analytical solution to the simplified model. In Section 4, the numerical methods are formulated. Section 5 focuses on validating the presented approach with direct numerical simulations. Section 6 presents a study of the efficiency of the energy recovery for different values of thermal losses. Finally, Section 7 gives some conclusions.

2. MODEL

In what follows, we introduce the mathematical model describing Electromagnetic-assisted Water Flooding (EMAWF), representing a two-dimensional extension of the model employed in Almeida et al., (2022)a, with EM energy absorption modeled through Maxwell's equations.

2.1. Energy Balance Equation

Following Almeida et al., (2022)a,b, Chen et al., (2006), Paz et al., (2017) we write the total energy balance equation as:

$$C_t(S_w)\partial_t\theta + C_l(S_w)\mathbf{u}\cdot\nabla\theta = K_t(S_w)\Delta\theta + H_l(\theta-\theta_0) + W, \tag{1}$$

where u represents the Darcy velocity. The coefficients in (1) can be described as the total specific heat of the system ($C_t(S_w)$), the total specific heat of the fluids ($C_l(S_w)$), the total thermal conductivity of the system ($K_t(S_w)$), thermal losses coefficient H_l, and the total source of electromagnetic energy (W). Following Almeida et al., (2022)a, these coefficients are given by:

$$C_t(S_w) = (\rho_w \phi S_w + \rho_s(1-\phi)c_s), \tag{2}$$

$$C_l(S_w) = (\rho_w c_w)S_w, \tag{3}$$

$$K_t(S_w) = \phi((K_w)S_w) + K_s(1-\phi)), \tag{4}$$

where K_β is the thermal conductivity, c_β is the specific heat, ρ_β is the density, sub-index $\beta = w,s$ refers to water, and solid phases. Following Paz et al., (2017), the coefficients above can be described as total specific heat of the system ($C_t(S_w)$), the total specific heat of the fluids ($C_l(S_w)$), the total thermal conductivity of the system ($K_t(S_w)$), and the total source of electromagnetic energy (W). We consider these three coefficients constant as in Almeida et al., (2022)a. Table 1 presents these parameter values estimated for $S_w = 1$.

The EM energy absorption (volumetric heat dissipation) function is given by

$$W = \frac{P_0}{2\pi h}\left(\frac{2\alpha}{r} + \frac{1}{r^2}\right)e^{-2\alpha(r-r_w)}, \tag{5}$$

where P_0 is the incidence power and $A = (2\pi r_w h)$ is the cross-sectional area normal to the radial direction of a right circular cylinder, with r_w the wellbore radius, h is the thickness (radial) and α is the attenuation factor (absorption coefficient). Its derivation is based on Maxwell's equations, encompassing Faraday's Law, Ampere's Law, Gauss's Laws, and uses the average Poynting vector; see Almeida et al., (2022)a, for details.

To estimate the heat transfer rate q [W] per unit of time within the material in the vertical direction we follow Eq. (1) combining it with Fourier's thermal conduction law, yielding:

$$q = K_t A d_z\theta, \tag{6}$$

where K_t is the thermal conductivity [W/(m K)], and A [m^2] is the area of the cross-section perpendicular to the flow's direction. By equating the total energy loss from (6) for a reservoir of dimensions $L \times L \times h$ (length, width, and height), using the linear thermal loss coefficient C_l, we obtain $H_l = K_t/h^2$.

Table 2: Physical parameters used in calculations, see Almeida et al., (2022)a, Paz et al., (2017), Sudiko (2014), Viswanath et al., (2007).

Sym	Physical quantity	Value	Unit (SI)
α	water EM energy absorption	4.185e-01	[1/m]
ε_0	vacuum electric permittivity	8.854e-12	[F/m]
ε	medium electric permittivity	81	[F/m]
θ_0	initial temperature	308.15	[K]
k_{rw}^0	final point water relative permeability	0.25	[-]
k	permeability	500	[mD]
μ_0	vacuum magnetic permeability	4πe-07	[H/m]
μ_r	medium magnetic permeability	1	[H/m]
ϕ	porosity	0.220	[-]
ρ_s	porous media density	2.650e03	[Kg/m^3]
ρ_w	water density	997	[Kg/m^3]
σ	medium conductivity	0.02	[S/m]
ω	angular frequency	$2\pi f$	[rad/s]
c_s	PM specific heat capacity	0.920e03	[J/Kg.K]
c_w	water specific heat capacity	4.2e03	[J/Kg.K]
f	frequency	2.45	[GHz]
h	reservoir thickness	1	[m]
r_w	wellbore radius	0.135	[m]
A	cross-sectional area of EM incidence	0.82	[m^2]
C_t	system specific heat	2.82	[MJ/m^3.K]
C_l	total fluid specific heat	4.19	[MJ/m^3.K]
K_t	total system thermal conduc.	1.92	[W/m.K]
$L_{1,2}$	reservoir length and width	40	[m]
K_s	PM thermal conductivity	2.30	[W/m.K]
K_w	water thermal conductivity	0.58	[W/m.K]
P	power of the EM emitter	250	[kW]

3. ANALYTICAL SOLUTIONS

We now seek analytical solutions for the simplified version of the Energy Balance Equation (1).

3.1. Dimensionless energy balance equation

First we rewrite the energy balance equation (1) in the dimensionless form by substituting

$$\tilde{t} = \frac{t}{t^*}, \quad \tilde{x} = \frac{x}{x^*}, \quad \tilde{y} = \frac{y}{y^*}, \quad \tilde{T} = \frac{\theta - \theta_0}{\Delta\theta^*}, \quad t^* = \frac{\phi L}{|u|}, \tag{7}$$

$$x^* = L_1, \quad y^* = L_2, \quad L = \max\{L_1, L_2\}, \quad \Delta\theta^* = \theta_0. \tag{8}$$

The resulting equation is:

$$\partial_t T + \nabla \cdot (vT) = b\Delta T + cT + dW, \tag{9}$$

where

$$b = \frac{K_{tot}\phi}{C_{tot}L|\mathbf{u}|}, \quad c = \frac{C_{ter}\phi L}{C_{tot}|\mathbf{u}|}, \quad d = \frac{K_{em}\phi L S_w}{C_{tot}|\mathbf{u}|\Delta\theta *}, \tag{10}$$

and

$$v = (v_1, v_2) = \left(\frac{C_{liq}\phi^2 u_1}{C_{tot}|\mathbf{u}|}, \frac{C_{liq}\phi^2 u_2}{C_{tot}|\mathbf{u}|}\right). \tag{11}$$

3.2. ENERGY BALANCE

To explore the energy balance relation (9), we consider the initial data $T(x, y, 0) = T_0 = 0$ in the rectangular domain $0 \leq x \leq \infty$ and $-\infty \leq y \leq \infty$. Applying the transformation Polyanin (2001) given by

$$T(x, y, t) = e^{(\psi t + \delta_1 x + \delta_2 y)} w(x, y, t), \tag{12}$$

with $\delta_1 = v_1/2b$, $\delta_2 = v_2/2b$, and $\psi = c - v_1^2/4b - v_2^2/4b$, the system (9) is rewritten as

$$\begin{cases} w_t(x, y, t) = b\Delta w(x, y, t) + \Phi(x, y, t), \\ w(x, y, 0) = f(x, y), \\ w(0, y, t) = g(y, t), \end{cases} \tag{13}$$

where $\Phi(t, x, y) = dWe^{-(\psi t + \delta_1 x + \delta_2 y)}$ and $f = T_0 e^{-(\delta_1 x + \delta_2 y)}$.

We solve (13) using Duhamel's principle, which involves solving a simplified system of equations.

$$\text{Case1:} \quad \begin{cases} w_t(x, y, t) = b\Delta w(x, y, t) + \Phi(x, y, t), \\ w(x, y, 0) = 0, \\ w(0, 0, t) = 0. \end{cases} \tag{14}$$

$$\text{Case2:} \quad \begin{cases} w_t(x, y, t) = b\Delta w(x, y, t), \\ w(x, y, 0) = f(x, y), \\ w(0, 0, t) = 0. \end{cases} \tag{15}$$

$$\text{Case3:} \quad \begin{cases} w_t(x, y, t) = b\Delta w(x, y, t), \\ w(x, y, 0) = 0, \\ w(0, y, t) = g(y, t). \end{cases} \tag{16}$$

The Duhamel method involves the individual resolution of each system and subsequently combining their solutions to achieve the complete solution, Evans (2010). In this process, it is imperative to carefully select the initial and boundary conditions for each resulting system, playing a crucial role in the comprehensive definition of the problem at each stage. While solving each system, specific mathematical methods and suitable techniques are applied to address the unique characteristics of each isolated component. The subsequent step involves the integration of the solutions from individual systems, resulting in the complete solution of Eq. (13). This approach proves particularly effective when dealing with dynamic or evolving problems, enabling a more accessible analysis by breaking down the complexity into more manageable parts. Following this procedure, it follows that

$$\begin{aligned} w(x, y, t) = \; & \int_0^\infty \int_{-\infty}^\infty f(\xi, \eta) G(x, y, \xi, \eta, t)\, d\eta\, d\xi \\ & + b \int_0^t \int_{-\infty}^\infty g(\eta, \tau) \left[\frac{\partial}{\partial \xi} G(x, y, \xi, \eta, t - \tau)\right]_{\xi = 0} d\eta\, d\tau \\ & + \int_0^t \int_0^\infty \int_{-\infty}^\infty \Phi(\xi, \eta, \tau) G(x, y, \xi, \eta, t - \tau)\, d\eta\, d\xi\, d\tau. \end{aligned} \tag{17}$$

Here Green's function associated with System (3.2) is given by:

$$\begin{aligned} & G(x, y, \xi, \eta, t) = \\ & \frac{1}{4\pi bt}\left[\exp\left(-\frac{(x-\xi)^2 + (y-\eta)^2}{4bt}\right) - \exp\left(-\frac{(x+\xi)^2 + (y-\eta)^2}{4bt}\right)\right]. \end{aligned} \tag{18}$$

4. NUMERICAL SOLUTIONS

To ensure the accuracy of the analytical estimates, we compare our results with their numerical counterpart. This comparison serves as a crucial step to ensure quality, ensuring that the theoretical foundations captured by analytical methods align harmoniously with the practical approximations derived from numerical techniques.

We employ a numerical approach utilizing the Galerkin Least-Squares Finite Element Method (GLS-FEM) (see Hughes et al., (1989)) for solving Equations (1). The GLS-FEM combines the accuracy of the standard Galerkin method with the stability of the Least Squares method, demonstrating exceptional efficiency, especially in scenarios characterized by high convection and low diffusion, Lube and Weiss (1995).

4.1. Galerkin Least-Squares Finite Element Method

We consider the boundary value problem (9) with boundary conditions given by:

$$-\mathbf{n}\cdot\nabla T = q(T-g_D)-g_N, \quad T\in\partial\Omega, \tag{19}$$

where Ω is a closed domain with boundary $\partial\Omega$, and the real numbers g_D, g_N, and q determine the boundary conditions used: Robin, Dirichlet, or Neumann. In the case defined in (13), the corresponding values are $g_D=0$, $g_N=0$, and $q=0$.

Following the GLS-FEM formulation, the discrete solution of Equation (9) is given by the linear combination of the test basis functions φ_i:

$$T_h = \xi_1(t)\varphi_1(x,y)+\xi_2(t)\varphi_2(x,y)+\ldots+\xi_l(t)\varphi_l(x,y), \tag{20}$$

where T_h is a piecewise function in the Hilbert space H^1, and $\xi_i=\xi_i(t)$ must be determined for $i\in\{1,2,3,\ldots,l\}$. Considering the differential operator $L=\partial_t+\nabla+\Delta$, the weak formulation for Eq. (9) is given by:

$$\begin{aligned}\langle LT_h,\varphi_i+\delta L\varphi_i\rangle &= \langle T_h+W,\varphi_i+\delta L\varphi_i\rangle,\\ \langle LT_h,\varphi_i\rangle+\delta\langle LT_h,L\varphi_i\rangle &= \langle T_h,\varphi_i\rangle+\langle W,\varphi_i\rangle+\delta\langle T_h,L\varphi_i\rangle+\delta\langle W,L\varphi_i\rangle,\end{aligned} \tag{21}$$

where the parameter δ is taken to increase the method's accuracy and varies according to the coefficients of Equation (9). Details about the method and how to estimate δ can be found in Hughes et al., (1989).

Finally, the ordinary differential equation is solved by using the implicit Euler method Strikwerda (1989).

5. VALIDATION OF THE ANALYTICAL APPROACH

We simulated the dimensionless Eq. (9) to validate the analytical estimates. As an illustration, we showcase a configuration with a horizontal well featuring one EM wave emitter; see Fig. 2. The EM emitter, located at position $(-2,20)$, possesses a power of P and is mathematically modeled by Eq. (5). The initial state of the reservoir is saturated with water at room temperature θ_0, and the parameter values as detailed in Table 1. Temperature considerations involve implementing a Dirichlet boundary condition on the well bore perimeter ($\theta(0,y,t)=\theta_0$) and Neumann null boundary conditions elsewhere, following the approach outlined in Alomair et al., (2014).

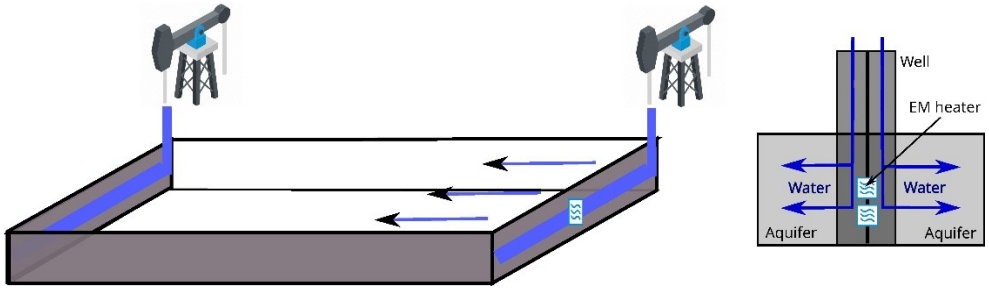

Figure 2: Schematic representation of the reservoir with two horizontal wells and one EM emitter used for estimate validation.

The analytical solution, detailed in Subsection 3.2, is plotted in Fig. 3. On the other hand, the numerical solution employs the discrete formulation outlined in Subsection 4.1 and is shown in Fig. 4.

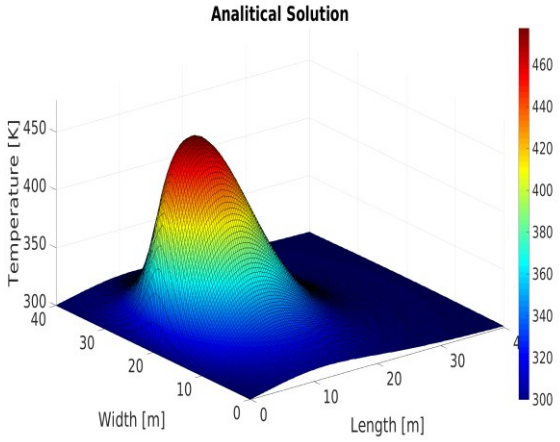

Figure 3: Analytical solution for temperature distribution along the reservoir after three months injection.

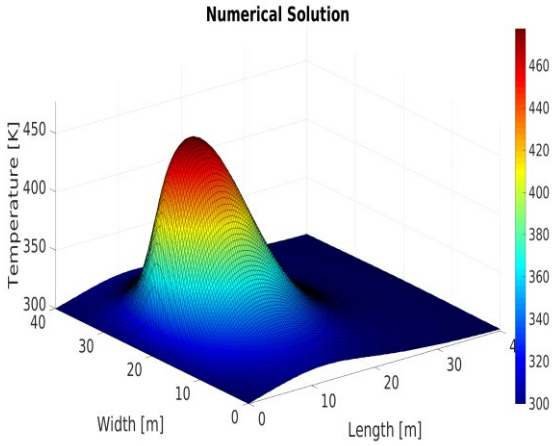

Figure 4: Numerical solution for temperature distribution along the reservoir after three months injection.

We refine the spatial mesh to assess the numerical implementation's convergence. Table 2 provides the distance between the numerical and analytical solutions using the standard L_2 norm. The relative distance is calculated as $(\| \theta^A - \theta^N \|)/\| \theta^A \| \times 100$, where θ^N represents the numerical solution, and θ^A corresponds to the analytical solution. Notably, reducing the diameter of the elements by half results in a fourfold increase in the total number of elements. The implemented algorithm exhibits quadratic behavior, aligning with the data presented in the table.

Table 2: Numerical method's convergence showing different meshes and corresponding errors for temperature field.

Mesh	312	1248
Relative Error	12,8%	2.7%

Examining analytical and numerical solutions for the temperature distribution along the reservoir after six months of injection has provided valuable insights into the convergence behavior of the numerical method across different mesh resolutions. Fig. 3 illustrates the analytical solution, while Fig. 4 showcases the numerical solution. Table 2 summarizes the results, indicating that for a mesh containing 312 triangles, the relative error concerning the analytical solution was 12.8%. Increasing the mesh complexity to 1248 triangles demonstrates a substantial improvement, with the relative error reduced to 2.7%. These findings underscore the sensitivity of the numerical solution to the mesh employed, showcasing the convergence of the method as the mesh is refined. The comparative plot between the analytical and numerical solutions represents the disparities and similarities between the results.

6. RESULTS

In this section, we discuss the process of storing and recovering energy generated by the electromagnetic emitter located within the aquifer. We consider three cases. In the first one, we do not consider thermal losses within the aquifer, thus setting the term $H_l = 0$ in Eq. 1. For the second one, we provide a realistic estimate for the thermal loss coefficient H_l. Finally, we consider an overestimate for H_l corresponding to more significant thermal losses.

We consider a cycle consisting of storage and energy recovery phases, each lasting 6 months. During the storage phase, water at ambient temperature (300 K) is continuously injected. A constant velocity field towards the water-injected well is assumed with horizontal well configuration; see Fig. 2. The energy recovery phase commences immediately after the storage period. In this phase, the injection flow is reversed; that is, the extraction well becomes the injector, and the previously used injector becomes the extractor. This premise is justified by observations in Figs. 5-10, where we can note that the heat profile near the injection well in phase 1 is higher. All the data used can be found in Table 1.

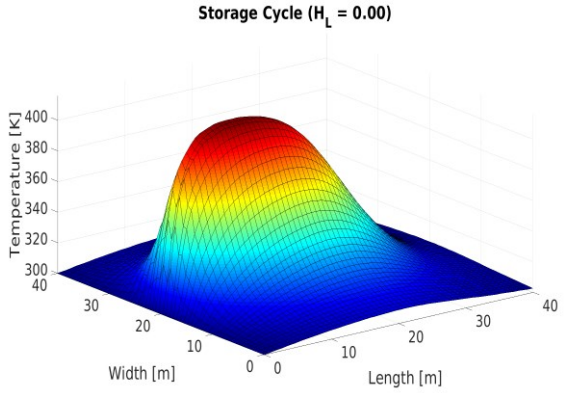

Figure 5: Analytical solution for temperature distribution along the reservoir after six months of energy storage disregarding thermal losses inside the reservoir.

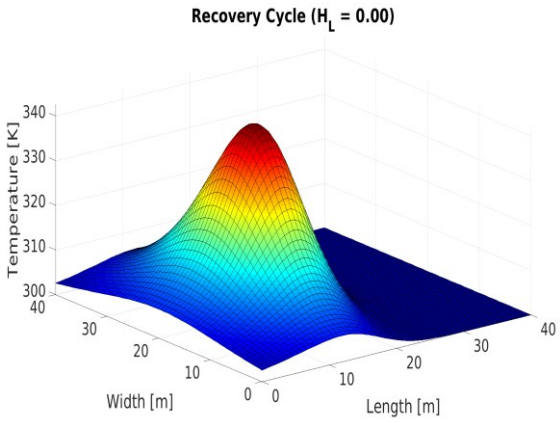

Figure 6: Analytical solution for temperature distribution along the reservoir after six months of energy recovery disregarding thermal losses inside the reservoir.

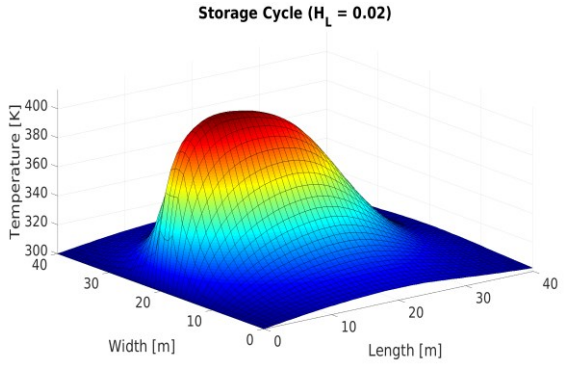

Figure 7: Analytical solution for temperature distribution along the reservoir after six months of energy storage with estimated thermal losses inside the reservoir.

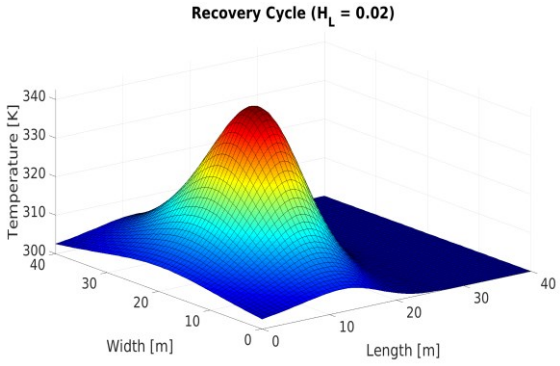

Figure 8: Analytical solution for temperature distribution along the reservoir after six months of energy recovery with estimated thermal losses inside the reservoir.

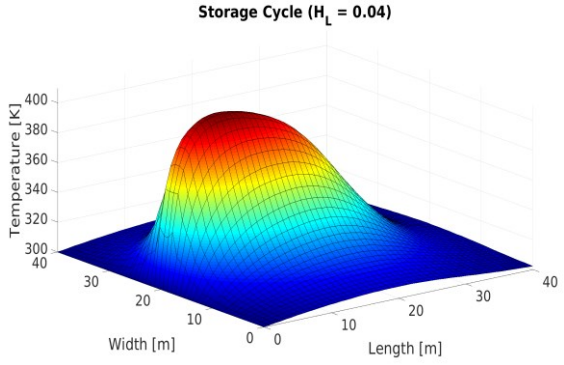

Figure 9: Analytical solution for temperature distribution along the reservoir after six months of energy storage with estimated thermal losses inside the reservoir five times greater.

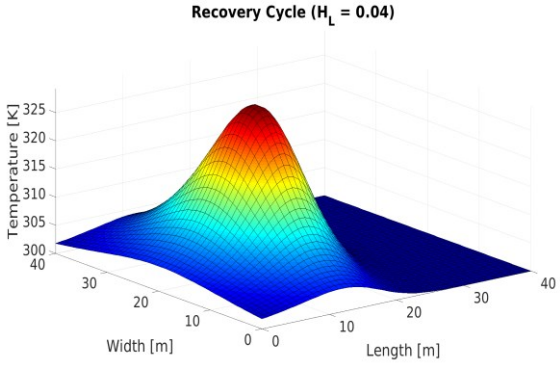

Figure 10: Analytical solution for temperature distribution along the reservoir after six months of energy recovery with estimated thermal losses inside the reservoir five times greater.

In Table 3, in Case 1, it was observed that by disregarding thermal losses ($H_l = 0$), the total amount of electromagnetic energy emitted and stored amounted to 134 GW. It is worth noting that, in this context, the aquifer fully absorbed all emitted electromagnetic energy during the storage phase, converting it into heat, as illustrated in Fig. 5. From this total, 100 GW could be recovered, justified by the fact that, at the end of the recovery phase, the aquifer retains a portion of the stored energy residually, as evidenced in Figure 6. The efficiency in this case is 74%.

For Case 2, where the estimated thermal loss coefficient was $H_l = 0.02$, there was a thermal loss in energy storage of 5 GW, as shown in Fig. 7. This loss, combined with residual loss, see Fig. 8, resulted in a lower recovery of the total stored energy (96 GW) and, consequently, an efficiency of only 68% in the cycle.

For Case 3, an evaluation was conducted with an overestimating thermal losses, doubling the coefficient ($H_l = 0.04$). In this scenario, the energy stored in the reservoir decreased to 122 GW. Upon analyzing the temperature profile, Fig. 9, it was found that the energy recovered at the end of the cycle was 78 GW, resulting in an efficiency of 58% of the total emitted. This considers both thermal and residual losses in the reservoir, as illustrated in Fig. 10.

Table 3: Efficiency in recovering the stored energy (injection per cycle $\approx$ 134 GW).

Thermal loss coeff.	Stored En.	Recovered En.	Efficiency
H_L = 0.00	134	100	74%
H_L = 0.02	129	92	68%
H_L = 0.04	122	78	58%

7. CONCLUSIONS

To further motivate the investigation of high-temperature energy storage (HT-ATES) in deep, high-temperature aquifers, we proposed simplifying the model presented in the literature, allowing an analytical solution taking into account the thermal losses. This solution is in agreement with numerical simulations. The following main conclusions can be drawn from this study:

- The obtained analytical solution evidence a stable thermal front spreading the energy through the aquifer with temperatures below the boiling point.
- The recovery efficiency, even with the overestimated heat losses, is up to 58% and agrees with the literature, see Almeida et al., (2022)a. The efficiency values are comparable with the low-temperature ATES, as reported in the literature.

ACKNOWLEDGEMENTS

G. C. was partly supported by CNPq grants 306970/2022-8, 405366/2021-3, and FAPEMIG grant APQ-00405-21.

REFERENCES

S. O. Almeida, G. Chapiro, and P. L. J. Zitha. Down-hole electromagnetic heating of deep aquifers for renewable energy storage. *Energies*, 15(11):3982, (2022).

S. O. Almeida, P. L. J. Zitha, and G. Chapiro. A method for analyzing electromagnetic heating assisted water flooding process for heavy oil recovery. *Transport in Porous Media*, 144:89-110, (2022).

O. Alomair, A. Elsharkawy, and H. Alkandari. A viscosity prediction model for kuwaiti heavy crude oils at elevated temperatures. *Journal of Petroleum Science and Engineering*, 120:102–110, (2014).

A. Bera and T. Babadagli. Status of electromagnetic heating for enhanced heavy oil/bitumen recovery and future prospects: A review. *Applied Energy*, 151:206 – 226, (2015).

A. Cerutti, M. Bandinelli, M. Bientinesi, L. Petarca, M. De Simoni, M. Manotti, and G. Maddinelli. A new technique for heavy oil recovery based on electromagnetic heating: System design and numerical modelling. *Chemical Engineering Transactions*, 32:1255–1260, (2013).

Z. Chen, G. Huan, and Y. Ma. *Computational Methods for Multiphase Flows in Porous Media (Computational Science and Engineering 2)*. SIAM, (2006).

A. B. Chhetri and M. R. Islam. A critical review of electromagnetic heating for enhanced oil recovery. *Petroleum Science and Technology*, 26(14):1619–1631, (2008).

J. S. Dickinson, N. Buik, M. C. Matthews, and A. Snijders. Aquifer thermal energy storage: theoretical and operational analysis. *Geotechnique*, 59(3):249–260, (2009).

R. Dorsey-Palmateer. Effects of wind power intermittency on generation and emissions. *The Electricity Journal*, 32(3):25 – 30, (2019).

S. Eskandari, S. M. Jalalalhosseini, and E. Mortezazadeh. Microwave heating as an enhanced oil recovery method - potentials and effective parameters. *Energy Sources, Part A: Recovery, Utilization, and Environmental Effects*, 37(7):742–749, (2015).

L. C. Evans. *Partial differential equations*. American Mathematical Society, (2010).

M. Z. Hasanvand and A. Golparvar. A critical review of improved oil recovery by electromagnetic heating. *Petroleum Science and Technology*, 32(6):631–637, (2014).

T. Hughes, P. Franca, and G. Hulbert. A new finite element formulation for computational fluid dynamics: Viii. the galerkin/least-squares method for advective-diffusive equations. *Computer Methods in Applied Mechanics and Engineering*, 73(2):173–189, (1989).

A. K. Jha, N. Joshi, and A Singh. Applicability and assessment of micro-wave assisted gravity drainage (mwagd) applications in mehsana heavy oil field. In *Proceedings of the SPE Heavy Oil Conference and Exhibition*, pages 11–14, (2011).

O. Kastner, B. Norden, S. Klapperer, S. Park, L. Urpi, M. Cacace, and G. Blocher. Thermal solar energy storage in jurassic aquifers in northeastern germany: A simulation study. *Renewable Energy*, 104:290–306, (2017).

D. Lau, N. Song, C. Hall, Y. Jiang, S. Lim, I. Perez-Wurfl, Z. Ouyang, and A. Lennon. Hybrid solar energy harvesting and storage devices: the promises and challenges. *Materials Today Energy*, 13:22–44, (2019).

G. Lube and D. Weiss. Stabilized finite element methods for singularly perturbed parabolic problems. *Applied Numerical Mathematics*, 17(4):431–459, (1995).

A. Mukhametshina and E. Martynov. Electromagnetic heating of heavy oil and bitumen: A review of experimental studies and field applications. *Journal of Petroleum Engineering*, 2013, (2013).

P. Z. S. Paz, T. H. Hollmann, E. Kermen, G. Chapiro, E. Slob, and P. L. J. Zitha. Em heating-stimulated water flooding for medium–heavy oil recovery. *Transport in Porous Media*, 119(1):57–75, (2017).

J. Pizarro and O. Trevisan. Electrical heating of oil reservoirs: numerical simulation and field test results.m*Journal of Petroleum Technology*, 42(10):1–320, (1990).

A. D. Polyanin. *Handbook of linear partial differential equations for engineers and scientists*. CRC press, 2 edition, (2001).

A. Sahni, M. Kumar, and R. B. Knapp. Electromagnetic heating methods for heavy oil reservoirs. In *SPE/AAPG Western Regional Meeting*. SPE, (2000).

S. Shafiai and A. Gohari. Conventional and electrical EOR review: the development trend of ultrasonic application in EOR. *Journal of Petroleum Exploration and Production Technology*, 10(7):2923–2945, (2020).

W. T. Sommer. *Modelling and monitoring of Aquifer Thermal Energy Storage: impacts of soil heterogeneity, thermal interference and bioremediation*. PhD thesis, Wageningen University, (2015).

C. J. Strikwerda. *Finite Difference Schemes and Partial Differencial Equations*. Wadsworth & Brooks, (1989).

M. N. O. Sudiko. *Elementes of Electromagnetics*. Oxford University Press, New York, 6 edition, (2014).

D. W. S. Tang and H. H. M. Rijnaarts. Dimensionless thermal efficiency analysis for aquifer thermal energy storage. *Water Resources Research*, 59(11):e2023WR035797, (2023).

D. S. Viswanath, T. K. Ghosh, D. H. L. Prasad, N. V. K. Dutt, and K. Y. Rani. *Viscosity of Liquids: Theory, Estimation, Experiment, and Data*. Springer Netherlands, (2007).